

Boosting Supervised Dehazing Methods via Bi-level Patch Reweighting

Xingyu Jiang¹, Hongkun Dou¹, Chengwei Fu¹, Bingquan Dai¹, Tianrun Xu²,
and Yue Deng^{1*}

¹ School of Astronautics, Beihang University
ydeng@buaa.edu.cn

² North China University of Technology

Abstract. Natural images can suffer from non-uniform haze distributions in different regions. However, this important fact is hardly considered in existing supervised dehazing methods, in which all training patches are accounted for equally in the loss design. These supervised methods may fail in making promising recoveries on some regions contaminated by heavy hazes. Therefore, for a more reasonable dehazing losses design, the varying importance of different training patches should be taken into account. Such rationale is exactly in line with the process of human learning that difficult concepts always require more practice in learning. To this end, we propose a bi-level dehazing (BILD) framework by designing an internal loop for weighted supervised dehazing and an external loop for training patch reweighting. With simple derivations, we show the gradients of BILD exhibit natural connections with policy gradient and can thus explain the BILD objective by the rewarding mechanism in reinforcement learning. The BILD is not a new dehazing method per se, it is better recognized as a flexible framework that can seamlessly work with general supervised dehazing approaches for their performance boosting.

Keywords: Single Image Dehazing, Bi-level Optimization, Visual Importance, Deep Learning

1 Introduction

Image dehazing has been widely discussed in the computer vision community and is vital for subsequent high-level tasks including image classification [23] and object detection [9]. Conventional dehazing algorithms can be categorized into prior-based approaches [20, 47] and data-driven approaches (*a.k.a.* supervised approaches)[34, 35, 45]. Prior-based dehazing models are mainly built upon the basic atmospheric scattering model [30, 31] with various physical assumptions imposed on image statistics. These prior-based models are more interpretable but can easily fail in real-world images where the assumed prior does not hold. Data-driven methods[12, 26, 43] tackle the dehazing problem from the view of supervised learning. Early supervised dehazing approaches [8, 23] mainly contribute

* Corresponding author

to designing learnable parametrized functions (*e.g.* a neural network) to replace some important modules (*e.g.* transmission maps) in the traditional atmospheric scattering model. Recent works [26, 32] show the potential to conduct supervised dehazing in an end-to-end manner by directly learning the hazy-to-clear mapping. Compared with the prior-based dehazing models, these data-driven approaches can better approximate the complex structure of the high-dimensional image manifold and hence achieve better performances on real-world images.



Fig. 1: The left shows non-uniform haze distributions in different regions. The degradation degree of red, blue and yellow patches varies from severe to mild. Compared with equally additive loss design (*e.g.* L1 loss in FFANet[32]), BILD framework performs much better in restoring dense-haze regions from both visualization and quantitative evaluations via PSNR/SSIM.

In the benchmark supervised dehazing protocol, large hazy images are always cropped into patches for subsequent dehazing learning[11, 12, 26, 32]. Such patch-level dehazing implementation can enhance the diversity of training samples, reduce the demands of hardware memory and improve the flexibility for parallelized training [7, 46]. Then, these patch-level losses are equally accumulated to define the image-level loss. While this equally accumulated loss is extensively used in existing works, we still suspect its reasonableness in the context of image dehazing. The haze distributions of real-world scenes are highly non-uniform [1, 3], making the cropped image patches vary greatly in degradation degrees (see the left column of Fig.1). When dehazing all patches with the same efforts, even the SOTA method (FFANet[32]) cannot effectively restore the seriously

contaminated patch from heavy haze (see the (b) row of Fig.1). Accordingly, the heterogeneity of these training patches should not be overlooked and their unique importances should be properly discriminated in the loss design.

To address the aforementioned challenges, we introduce a simple patch reweighting strategy by assigning different importance weights to different patches. In this way, the image-level loss is becoming a weighted summation of the individual losses from its containing patches. Such patch-level reweighting is intuitive and exactly mimic the behaviour of human learning, that people always invest more learning efforts on valuable matters[37, 39, 42]. As a whole, we design a bi-level dehazing(BILD) framework to enable automatically patch reweighting by monitoring the learned dehazing performances on some out-of-sample data. In details, the internal loop of BILD is trained for weighted supervised dehazing with in-sample training patches; and the external loop utilizes out-of-sample patches from validation set for training patch reweighting. The in-sample training and out-of-sample validating strategy can ultimately enhance the generalization ability of the trained dehazing machines.

With simple derivatives, we further bridge our BILD model with the policy gradient and interpret its objective function from max-entropy reinforcement learning[18]. The dehazing performances of the same algorithm can be non-trivially improved by BILD (as observed from the (c) row in Fig.1), especially for those hard patches. While only the FFANet[32] was used as a showcase here, we emphasized that the BILD is general enough to improve other supervised dehazing methods, by simply integrating their respective objectives into BILD’s internal loop.

We summarize the main contributions as three-fold:

- We propose bi-level dehazing (BILD) — a general framework that is compatible with various supervised dehazing approaches for performance boosting, especially in restoring seriously degraded regions.
- We introduce the reweighting and validating concepts into dehazing tasks for improving their generalizations in dehazing new images with non-uniform haze distributions.
- We uncover the natural connections of our BILD model with max-entropy reinforcement learning, enhancing the interpretability of the whole learning process from the novel view of agent-environment interactions.

2 Related work

Single Image Dehazing. All along, single image dehazing is viewed as a highly ill-posed problem, which requires extra prior information or constraints. To tackle this problem, existing single image dehazing methods can be divided into two categories: the prior-based methods[6, 20, 28, 47] and the data-driven methods [11, 33–36].

Most prior-based approaches employ novel physical assumptions (*e.g.* DCP [20], CAP[47], NLD[6]) to estimate the transmission map and ambient light[5] in atmospheric scattering model[30, 31], which can explicitly recover a clear image from haze. For instance, He *et al.* [20] notice pixels (at least one channel) tend to zero on non-sky regions. Berman *et al.* [6] observe pixel colors of the whole scene can be well clustered to hundreds of distinct colors. These prior-based methods show nice statistical properties in specific scenes, but can easily fail in real-world images where the physical assumptions do not hold.

Recently, data-driven supervised dehazing methods have been proposed to overcome shortcomings of traditional prior-based methods, with advances in deep learning and the establishment of large-scale datasets[24, 2, 1]. Early supervised dehazing approaches [8, 23, 45] design learnable neural networks to estimate the transmission map and ambient light. In [8], DehazeNet designs a three-layer CNN with BReLU activation function to estimate transmission map. Recent works trigger a great impact on supervised dehazing by learning the hazy-to-clear mapping in an end-to-end manner. The GridDehazeNet[26] designs an attention-based multi-scale network to directly recover haze-free images and introduces perception loss in objective. In [43], AECRNet develops an autoencoder-like dehazing network with a novel contrastive regularization. Although great advances have been made in network architecture and loss design, samples of different importances are equally accounted in loss computation. In this work, by introducing the idea of visual importance, we design a weighted loss function based on traditional L1/L2 loss and employ bi-level optimization strategy to optimize it.

Bi-level optimization. Bi-level optimization is committed to optimizing another set of parameters other than target network parameters, which describes higher-level elements related to training neural networks[37]. Wu *et al.*[44] trains a task scheduler for sequential learning to better assist the main task. Wang *et al.*[42] uses bi-level optimization to help with data selection. Sun *et al.*[39] designs an efficient data sampling schedule for learning a robust sampling strategy. In addition, the bi-level optimization can also be used to optimize the graph structure and embedding[14], ensemble model[25, 27], data auto-augment [10, 29, 41] and search network structure[4, 15]. In this work, inspired by the idea of maximum entropy in reinforcement learning[19, 17], we design the entropy regular term in external loop to alleviate the phenomenon of weight concentration in one batch, which can enhance the stability of training process. To our best knowledge, we are the first paper to combine bi-level optimization with visual importance in the field of image restoration and our BILD framework can boost the performance of supervised dehazing methods well beyond SOTA.

3 Bi-level Dehazing Framework

3.1 Patch reweighting

In supervised dehazing training, small patches x are cropped from the large hazy image and are fed into an arbitrary dehazing neural network $f_d(\cdot; \theta)$ param-

etrized by θ . The dehazing performance on this single patch can be quantified by counting the differences between the dehazed image with its corresponding ground truth clean image y under some proper loss L , *e.g.* the L_1 norm:

$$\ell(x, y; \theta) = L(f_d(x; \theta), y) \quad (1)$$

Then, these single-patch-losses are equally accumulated forming the global loss function J_e on the training set \mathcal{D}_t :

$$J_e(\mathcal{D}_t; \theta) = \mathbb{E}_{(x,y) \sim \mathcal{D}_t} \ell(x, y; \theta) \quad (2)$$

The additive loss J_e implies that different patches are treated equally in training, although they can suffer from very different degrees of degradation or with very diverse pixel distributions. While J_e has already been a benchmark loss function used in most existing supervised dehazing methods, we still consider it is not ideal for the discussed dehazing tasks because the haze distribution on the same scene can be highly heterogeneous (see Fig.1). Therefore, the values of different training samples should be properly weighted and exploited in the loss design. To this end, we introduce a more reasonable dehazing loss by the intuitive reweighting mechanism:

$$J_w(\mathcal{D}_t; \phi, \theta) = \mathbb{E}_{(x,y) \sim \mathcal{D}_t} w(x, y; \phi) \ell(x, y; \theta) \quad (3)$$

where $w(x, y; \phi) = f_w(x, y; \phi)$ is the output of the weighting neural network $f_w(\cdot; \phi)$ with (x, y) as input. We remark here that although we have fully emphasized the importance of patch reweighting, the underlying weighting mechanism is still unknown. For instance, for two patches that vary in backgrounds and illuminations, there is no concrete prior to inform us which patch should be weighed heavier than the other in the loss function. Accordingly, rather than heuristic weighting, we opt to adopt the parametrized weighting mechanism that can automatically assess the importance of each training patch through a learnable neural network $f_w(\cdot; \psi)$.

3.2 Bi-level dehazing framework

While the aforementioned parametrized weighting concept is simple, it yields a highly under-determined and non-convex objective function coupled with two unknown neural networks. Without extra constraints, the direct minimization of $J_w(\mathcal{D}_t; \phi, \theta)$ on the training set can easily lead to a trivial solution. In this case, the reweighting neural network $f_w(\cdot; \psi)$ may intend to assign (near) zero weights to all patches and hence totally mute the functions of the dehazing network (see the multiplications between the weight term and dehazing loss term in J_w in Eq.3). To avoid such trivial solution, extra constraints or guiding information should be imposed to restrict the feasibility of the learned results. In this work, inspired by recent works [16, 37, 39, 41, 42], we consider enforcing the feasibility of the learned results by monitoring the dehazing networks' performances on a

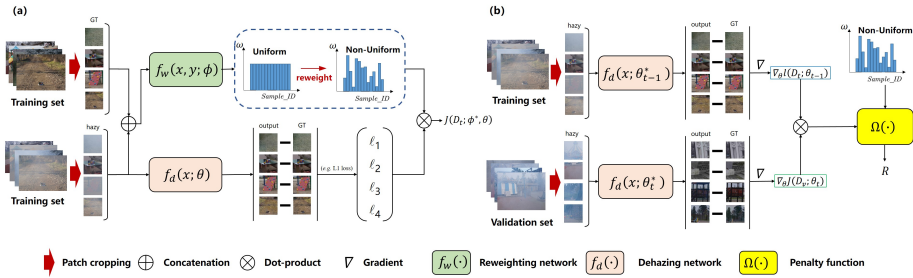


Fig. 2: The optimization process of the BILD framework, which consists of two loops. (a) The computational flow of internal weighted supervised dehazing loop. Patches from training set are fed into reweighting and dehazing network, respectively, to generate patch-wise weights and reconstruction loss of restored images and ground-truth. Then, the dot-product of the two outputs yields the objective function of internal loop. (b) The computational flow of external patch reweighting loop. Patches from training and validation set are respectively fed into dehazing networks of two consecutive iterations to obtain the gradient of reconstruction loss (e.g. L1 loss). Then, the combination of the saved gradient and penalty function constitutes the key reward for external loop updating (see eq.6 and 7)

new validation set $\mathcal{D}_v, \mathcal{D}_t \cap \mathcal{D}_v = \emptyset$ (see related ablation study in section 4.3). With this objective, the whole learning process is subject to the following bi-level dehazing (BILD) optimization:

$$\begin{aligned} \min_{\phi} \quad & J_e(\mathcal{D}_v; \theta^*(\phi)) + \alpha \Omega(\mathbf{w}) \\ \text{s.t.} \quad & \theta^*(\phi) = \arg \min_{\theta} J_w(\mathcal{D}_t; \phi, \theta) \end{aligned} \quad (4)$$

The above bi-level optimization is composed of the internal loop in the constraint and the external loop in the objective function. The internal loop minimizes the empirical error of the training set under guidances of the patch-wise weight provided by the external loop. The external loop trades off the generalization error and penalty term with a hyper-parameter α . The generalization error is obtained by evaluating the current suboptimal dehazing network on the keep-out validation data and the penalty term quantify the structure of \mathbf{w} with a function $\Omega(\mathbf{w})$, where $\mathbf{w} = [w(x_0, y_0; \phi), w(x_1, y_1; \phi), \dots, w(x_n, y_n; \phi)]^T$ and n is the number of training patches in a batch. The most intuitive penalty function can be used here is the entropy term that encourages the learned patch-wise weight not only to concentrate on a small number of training patches.

The primary advantage of building up the external loop is to enhance our dehazing models' generalization ability outside the training samples. Loosely speaking, the external loop learns to generate a set of reasonable weights $w(\cdot; \phi)$ that can guide the internal optimization converging to better solutions with enhanced generalization ability. The enhanced generalization ability covers two

angles including better generalization to out-of-sample new images (granted by the validating mechanism in the external loop) and better generalization to various training patches (granted by the weighting mechanism in the internal loop).

The parameter (θ) is only involved in the internal loop and can be easily updated with typical gradient descending approaches on a sampled batch with n patches,

$$\theta_t \leftarrow \theta_{t-1} - \eta_1 \nabla_{\theta} \sum_{i=0}^n w(x_i, y_i; \phi) \ell(x_i, y_i; \theta) \quad (5)$$

The major difficulty of the BILD optimization stems from the external loop to learn parameter ϕ for the reweighting neural network. As witnessed in Eq.4, ϕ is coupled into θ and its gradient can be derived by applying the chain rule (detailed derivation is available in supplement):

$$\begin{aligned} & \nabla_{\phi} (J_e(\mathcal{D}_v; \theta_t) + \alpha \Omega(\mathbf{w})) \\ &= - \sum_i \nabla_{\phi} \log w(x_i, y_i; \phi) \\ & \quad \cdot \underbrace{w(x_i, y_i; \phi) \left[\nabla_{\theta} J_e(\mathcal{D}_v; \theta_t)^{\top} \nabla_{\theta} \ell(x_i, y_i; \theta_{t-1}) - \alpha \frac{\partial \Omega(\mathbf{w})}{\partial w(x_i, y_i; \phi)} \right]}_{R_i} \end{aligned} \quad (6)$$

The above equation is an approximate solution for external loop updating. The R_i can be regarded as the feedback of internal dehazing loop to patch reweighting neural network (As is shown in Fig.2b). Here, we use entropy $\mathcal{H}(\mathbf{w})$ as the regular term $\Omega(\mathbf{w})$, preventing over concentration of sample weight. Thus, we get the update rule of ϕ ,

$$\phi_t \leftarrow \phi_{t-1} + \eta_2 \sum_{i=0}^n \frac{1}{n} R_i \cdot \nabla_{\phi} \log w(x_i, y_i; \phi) \quad (7)$$

According to the updating rules based on Eq.5 and 7, we alternately optimize two sets of parameters as in Algorithm.1. It is worth noting that BILD can be used to improve various supervised dehazing network or be integrated with other alternative losses, which will be extended in the experimental part.

3.3 Relationship with RL

The updating rule for ϕ in Eq.7 resembles the general form of policy gradient approaches used in REINFORCE algorithm [38, 40]. Then, we can interpret the coupled bi-level optimization from the view of reinforcement learning. In this context, the iterative interactions between the external and internal loops are well illustrated as agent-environment interactions. In detail, the external patch reweighting network is an agent, learning to perform actions (generating weights)

Algorithm 1: Bi-level dehazing framework

Input: Parameters of dehazing network θ ; parameters of reweighting network ϕ ; trainset \mathcal{D}_t ; validset \mathcal{D}_v

Output: θ^*

- 1 **for** $epoch = 1$ **to** max_epoch_nums **do**
- 2 **for** \mathcal{B} **in** \mathcal{D}_t **do**
- 3 Crop \mathcal{B} randomly into $\{x_i, y_i\}_{i=1,2,\dots,n}$
- 4 Fix ϕ and update θ via eq.5
- 5 Evaluation on \mathcal{D}_v and calculate R_i
- 6 Fix θ and update ϕ via eq.7
- 7 **end**
- 8 **end**

to the environment. After getting the action from the agent, three sequential implementations will be activated in the environment including 1) updating the dehazing neural network with the guidance of the current action (weight), 2) evaluate the updated dehazing net on the validation set and 3) generate the reward R by synchronizing the training performance, validating performance and the quality of the current action by the formulation defined in Eq.6. As observed from the first term in reward R_i , the environment intends to feedback a positive reward when the inner product between $\nabla_{\theta} J_e(\mathcal{D}_v; \theta_t)$ (from validation set) and $\nabla_{\theta} \ell(x_i, y_i; \theta_{t-1})$ (defined on training set) is close enough and vice versa(see eq.6). Moreover, when using the entropy $\mathcal{H}(\cdot)$ to realize the penalty $\Omega(\cdot)$ in R_i , we retain the same reward penalty mechanism as defined in the maximum entropy reinforcement learning[19, 17] that can encourage the actor to explore more adequately in the action space.

4 Experimental Results

4.1 Training, Validation and Testing Dataset

We evaluate the proposed framework on both synthetic datasets and real-world datasets against the state-of-the-art methods. The RESIDE [24] is a widely used synthetic dataset, which contains both indoor and outdoor synthetic images. To evaluate the effectiveness of our framework on synthetic hazy scenes, the RESIDE dataset is divided into three parts: training, validation and testing, respectively in indoor and outdoor datasets. For training, we randomly select 5000 indoor hazy/clear pairs from Indoor Training Set (ITS) and 5000 outdoor pairs from Outdoor Training Set (OTS). For validation, we hold out 10% of the training part. For testing, Synthetic Objective Testing Set (SOTS) is adopted, which contains 500 indoor and 500 outdoor hazy images. As for real-world hazy scenes, O-HAZE [2] and NH-HAZE [1, 3] datasets are adopted and each dataset provides training sets, validation sets and testing sets. More details can be found in the supplement.

Table 1: Quantitative evaluations on the synthetic datasets and real-world datasets in terms of PSNR and SSIM.

Method	SOTS [24]				O-HAZE [2]		NH-HAZE [1]	
	indoor		outdoor		PSNR \uparrow	SSIM \uparrow	PSNR \uparrow	SSIM \uparrow
	PSNR \uparrow	SSIM \uparrow	PSNR \uparrow	SSIM \uparrow				
(TPAMI'10) DCP [20]	16.62	0.8179	19.13	0.8148	15.87	0.6310	12.36	0.4448
(ICCV'13) BCCR [28]	17.04	0.7853	15.51	0.7914	14.43	0.5825	13.12	0.4831
(TIP'15) CAP [47]	18.97	0.8148	18.14	0.7585	15.36	0.5785	12.39	0.3753
(TPAMI'18) NLD [6]	17.29	0.7767	17.97	0.8194	15.34	0.5891	12.23	0.4823
(TIP'16) DehazeNet [8]	20.56	0.7954	–	–	–	–	–	–
(ICCV'17) AODNet [23]	19.04	0.8215	22.43	0.9022	18.07	0.6517	16.93	0.5717
(ICCV'19) GridDehazeNet [26]	28.22	0.9691	27.53	0.9583	22.11	0.7097	17.22	0.5921
(CVPR'20) MSBDN [12]	28.66	0.9515	26.94	0.9107	22.99	0.6927	17.97	0.6072
(AAAI'20) FFANet [32]	31.44	0.9728	30.50	0.9718	24.13	0.7438	18.04	0.6236
DehazeNet + BILD	21.15	0.8509	–	–	–	–	–	–
AODNet + BILD	19.53	0.8303	24.44	0.9216	20.81	0.6706	17.36	0.5779
GridDehazeNet + BILD	28.87	0.9765	27.93	0.9649	22.43	0.7242	17.97	0.6075
MSBDN + BILD	29.69	0.9596	27.03	0.9113	23.54	0.6954	18.14	0.6201
FFANet + BILD	32.14	0.9747	31.22	0.9760	24.91	0.7552	19.13	0.6439

4.2 Implementation Details

Our BILD framework consists of internal and external networks and is optimized by alternative training. Adam optimizer with β_1 and β_2 equal to 0.9 and 0.999 is used to train the two networks with a batch size of 10, respectively. The initial learning rate of the internal network is set as 10^{-4} with the external network set as 10^{-1} . The training epoch is set to 150 in total. All training models are trained on training set and verified on validation set. We choose the best model on the validation as the final model to evaluate its performance on the test set. All experiments are implemented by PyTorch 1.7.1 with one NVIDIA 3090 GPU.

Considering image sizes of different datasets and GPU memory, following [32, 12] work: for RESIDE dataset, which image size is 640×480 , we randomly crop size 240×240 patches as networks' input; for O-HAZE and NH-HAZE, where image size is 1600×1200 or even 4599×3632 , we randomly crop size 800×800 as input. Following [46] work, due to GridDehazeNet, FFA, MSBDN cannot process 4K images in O-HAZE, we adopt the downsample-dehazing-upsample (DDU) [46] strategy to solve this problem. Also for DCP[20], the window size is set to 15×15 for less time cost [46]. See supplementary materials for network architecture and more details.

4.3 Performance Results and Ablation Analysis

We evaluate the proposed BILD framework against SOTA methods based on the physics prior and supervised data-driven learning. The metrics PSNR and SSIM are adopted and all dehazing methods are retrained on the selected training, validation and testing datasets.

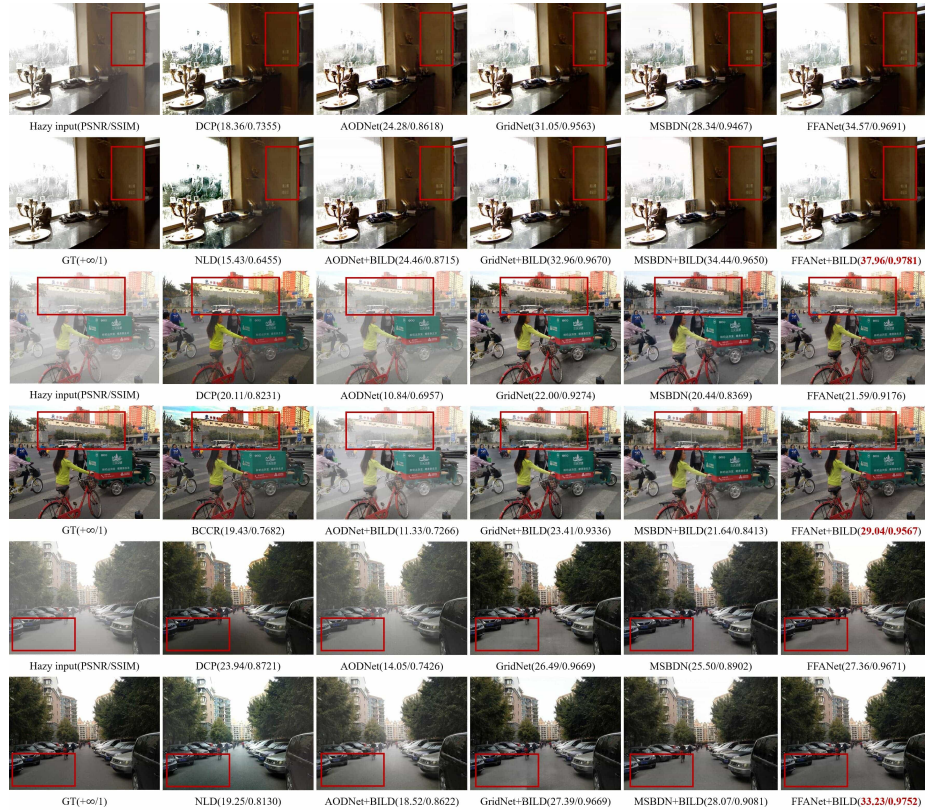


Fig. 3: Visual comparisons on the SOTS dataset. More examples can be found in supplement. Zoom in for best view.

Results on Synthetic Dataset. The first four columns of Tab.1 show the quantitative results on SOTS[24]. Our BILD framework improves the performances of SOTA methods to varying degrees. As shown, FFANet + BILD obtains the highest PSNR and GridDehazeNet + BILD obtains the highest SSIM on the indoor part. Meanwhile, FFANet + BILD obtains the highest PSNR and SSIM on the outdoor part. We also compare the qualitative results(see Fig.3). We can observe that physics-prior dehazing methods (DCP[20], BCCR[28], CAP[47] and NLD[6]) tend to over-darken or over-enhance the hazy image and are unable to remove dense haze. Compared to physics-prior methods, the supervised dehazing methods achieve better visual quality. However, the quality of DehazeNet is greatly affected by the estimation of ambient light and others (*e.g.* GridDehazeNet, MSBDN and FFANet) cannot remove haze uniformly: some regions close to the ground-truth but some regions still remain hazy. Our method restores the hazy images more uniformly and removes haze more thoroughly at patch-level(see red box in Fig.3).



Fig. 4: Visual comparisons on the O-HAZE dataset. Zoom in for best view.

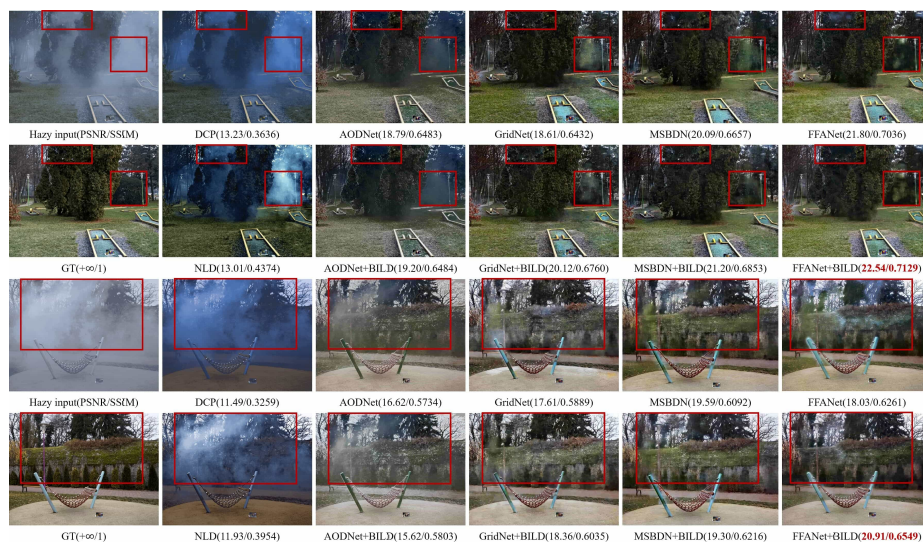


Fig. 5: Visual comparisons on the NH-HAZE dataset. Zoom in for best view.

Results on Real-world Dataset. The last four columns of Tab.1 demonstrate the quantitative results on the O-HAZE[2] and NH-HAZE dataset[1]. As shown, on O-HAZE dataset[2], our FFANet + BILD framework obtains the highest PSNR and SSIM and achieves the gain with 0.78 dB and 0.0114 in terms of PSNR and SSIM compared to FFANet[32] method. On NH-HAZE dataset[1], our FFANet + BILD framework obtains the highest PSNR and SSIM and achieves the gain with 1.09 dB and 0.0203 in terms of PSNR and SSIM compared to FFANet[32] method. The qualitative results are presented in Figs.4 and 5. As shown, our BILD + SOTA methods perform better color restoration (particularly with AODNet[23]) and better patch-level haze removal (see Figs.4 and 5). The physics-prior methods (DCP[20], BCCR[28], CAP[47] and NLD[6]) and AODNet[23] suffer from serious color distortion. Besides, GridDehazeNet [26], MSBDN[12] and FFANet[32] still have some residual haze in dense-haze regions(see red box in Figs.4 and 5).

Table 2: Results of applying our framework into SOTA methods.

Method	SOTS-indoor[24]		O-HAZE[2]	
	PSNR	SSIM	PSNR	SSIM
DehazeNet + BILD	↑0.59	↑0.0555	–	–
AODNet + BILD	↑0.49	↑0.0088	↑2.74	↑0.0189
GridDehazeNet + BILD	↑0.65	↑0.0079	↑0.32	↑0.0145
MSBDN + BILD	↑1.03	↑0.0081	↑0.55	↑0.0027
FFANet + BILD	↑0.70	↑0.0019	↑0.78	↑0.0114

Ablation Analysis of BILD. We apply the BILD framework to various SOTA methods to evaluate its effectiveness[8, 23, 26, 32]. As presented in Tab.2, our BILD framework can improve the performance of SOTA methods to varying degrees. Furthermore, the BILD framework cannot increase the additional parameters for the internal supervised dehazing network, since the external patch reweighing network is just used for training and can be removed for testing. Experiment results also show that the BILD framework can further increase supervised dehazing network training efficiency for performance boosting, as shown in Fig.6.

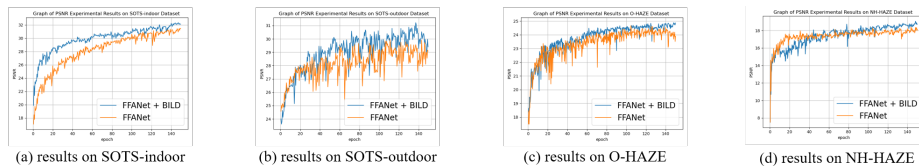


Fig. 6: Graph of PSNR with/without BILD framework during training process.

Table 3: Comparison of the effectiveness with training set and validation set in external loop.

Method	SOTS: indoor	
	PSNR	SSIM
AODNet[23]	19.04	0.8215
GridDehazeNet[26]	28.22	0.9691
MSBDN[12]	28.66	0.9515
FFANet[32]	31.44	0.9728
AODNet + training set	19.33	0.8239
GridDehazeNet + training set	28.68	0.9704
MSBDN + training set	28.92	0.9518
FFANet + training set	31.53	0.9739
AODNet + validation set	19.53	0.8303
GridDehazeNet + validation set	28.87	0.9765
MSBDN + validation set	29.69	0.9596
FFANet + validation set	32.14	0.9747

We meanwhile consider the effect of validation set in external patch reweighting loop. For better comparisons, we design the corresponding ablation experiments: 1) without external reweighting loop(see the first four rows in Tab.3), 2) with external reweighting loop but objective function is defined on training set(see the middle four rows in Tab.3) and 3) with external reweighting loop and objective function is defined on validation set(see the last four rows in Tab.3). We conduct the same training setting for all experiments and considering the volume of data, we integrate the validation set into the training set for the experiments of "BILD + training set". The results are summarized in Tab.3. Our "BILD + validation set" outperforms "BILD + training set" and baseline, which shows the effectiveness with validation set in external loop.

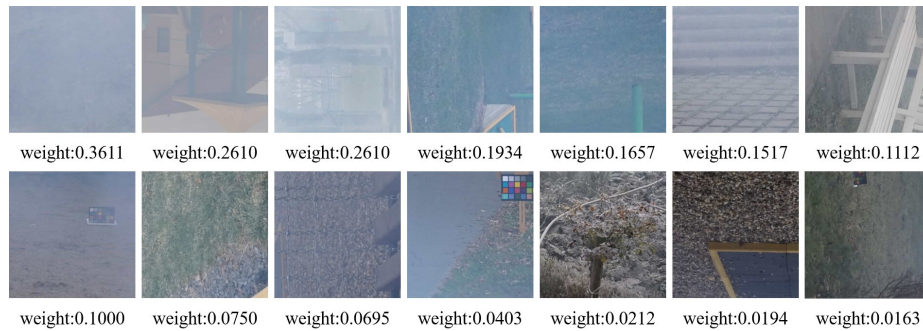


Fig. 7: The experimental results of patch reweighting. More examples can be found in supplement.

4.4 Patch Reweighting and Additional Experiment

Fig.7 illustrates the learned importance of each patch generated by the external patch reweighing loop. In general, the dense-haze patches have more learning weights and the light-haze patches have less learning weights, which is in line with our intention. Meanwhile, experimental results show that the complex background and illumination will also encourage more learning weight (see Fig.7).

Table 4: Results of applying our framework on full ITS dataset.

Method	full-indoor[24]	
	PSNR	SSIM
(ICCV'19) GridDehazeNet[26]	32.16	0.9836
(ECCV'20) FDU[13]	32.68	0.9760
(CVPR'20) MSBDN[12]	33.79	0.9840
(CVPR'20) KDDN[21]	34.72	0.9845
(AAAI'20) FFANet[32]	36.39	0.9886
(CVPR'21)AECRNet[43]	37.17	0.9901
FFANet + BILD	38.58	0.9921

Considering the training time cost and empirical partition ratio of training, validation and testing sets [22, 42], we select a subset from RESIDE dataset [24] for supervised dehazing, which may suffer from overfitting of the training set. As a complement, we conduct additional experiments on full ITS dataset[24] to evaluate the effectiveness of our BILD framework, in which FFANet is adopted as the supervised dehazing network. Experimental results show our BILD framework achieves the best performance compared with SOTA methods(see Tab.4).

5 Conclusion

In this paper, we propose a bi-level supervised dehazing framework(*e.g.* BILD), which is composed of two mutually coupled loops. The internal loop solves the weighted supervised dehazing optimization with the known patch-wise weights provided by the external loop. The external loop evaluates the current dehazing network (obtained from internal loop) on validated samples and, accordingly, generates a new set of structured weights to guide the supervised dehazing in the internal loop. The combination of the two alternative loops strengthens the robustness of supervised dehazing process. The BILD framework is compatible with general supervised dehazing methods and extensive experiments demonstrate our BILD framework boosts the performances of SOTA methods to varying degrees on synthetic and real-world datasets.

Acknowledgement: This research is supported by National Natural Science Foundation of China (Grant No.62031001, Grant No.61971020), National Key Research and Development Program of China (No.2020AAA0105502).

References

1. Ancuti, C.O., Ancuti, C., Timofte, R.: NH-HAZE: an image dehazing benchmark with non-homogeneous hazy and haze-free images. In: CVPRW (2020)
2. Ancuti, C.O., Ancuti, C., Timofte, R., Vleeschouwer, C.D.: O-haze: a dehazing benchmark with real hazy and haze-free outdoor images. In: CVPRW (2018)
3. Ancuti, C.O., Ancuti, C., Vasluianu, F.A., Timofte, R., et al.: NTIRE 2020 challenge on nonhomogeneous dehazing. In: CVPRW (2020)
4. Baker, B., Gupta, O., Naik, N., Raskar, R.: Designing neural network architectures using reinforcement learning. arXiv preprint arXiv:1611.02167 (2016)
5. Berman, D., Treibitz, T., Avidan, S.: Air-light estimation using haze-lines. In: ICCP. pp. 1–9 (2017)
6. Berman, D., Treibitz, T., Avidan, S.: Single image dehazing using haze-lines. IEEE TPAMI **42**(3), 720–734 (2018)
7. Bochkovskiy, A., Wang, C.Y., Liao, H.Y.M.: Yolov4: Optimal speed and accuracy of object detection. arXiv preprint arXiv:2004.10934 (2020)
8. Cai, B., Xu, X., Jia, K., Qing, C., Tao, D.: Dehazenet: An end-to-end system for single image haze removal. IEEE TIP **25**(11), 5187–5198 (2016)
9. Chen, Y., Li, W., Sakaridis, C., Dai, D., Van Gool, L.: Domain adaptive faster r-cnn for object detection in the wild. In: CVPR. pp. 3339–3348 (2018)
10. Cubuk, E.D., Zoph, B., Mane, D., Vasudevan, V., Le, Q.V.: Autoaugment: Learning augmentation strategies from data. In: CVPR. pp. 113–123 (2019)
11. Deng, Z., Zhu, L., Hu, X., Fu, C.W., Xu, X., Zhang, Q., Qin, J., Heng, P.A.: Deep multi-model fusion for single-image dehazing. In: ICCV. pp. 2453–2462 (2019)
12. Dong, H., Pan, J., Xiang, L., Hu, Z., Zhang, X., Wang, F., Yang, M.H.: Multi-scale boosted dehazing network with dense feature fusion. In: CVPR. pp. 2157–2167 (2020)
13. Dong, J., Pan, J.: Physics-based feature dehazing networks. In: ECCV. pp. 188–204 (2020)
14. Franceschi, L., Niepert, M., Pontil, M., He, X.: Learning discrete structures for graph neural networks. In: ICML. pp. 1972–1982 (2019)
15. Gao, Y., Yang, H., Zhang, P., Zhou, C., Hu, Y.: Graphnas: Graph neural architecture search with reinforcement learning. arXiv preprint arXiv:1904.09981 (2019)
16. Grazi, R., Franceschi, L., Pontil, M., Salzo, S.: On the iteration complexity of hypergradient computation. In: ICML. pp. 3748–3758 (2020)
17. Haarnoja, T., Tang, H., Abbeel, P., Levine, S.: Reinforcement learning with deep energy-based policies. In: ICML. pp. 1352–1361 (2017)
18. Haarnoja, T., Zhou, A., Abbeel, P., Levine, S.: Soft actor-critic: Off-policy maximum entropy deep reinforcement learning with a stochastic actor. In: ICML. pp. 1861–1870 (2018)
19. Haarnoja, T., Zhou, A., Hartikainen, K., Tucker, G., Ha, S., Tan, J., Kumar, V., Zhu, H., Gupta, A., Abbeel, P., et al.: Soft actor-critic algorithms and applications. arXiv preprint arXiv:1812.05905 (2018)
20. He, K., Sun, J., Tang, X.: Single image haze removal using dark channel prior. IEEE TPAMI **33**(12), 2341–2353 (2010)
21. Hong, M., Xie, Y., Li, C., Qu, Y.: Distilling image dehazing with heterogeneous task imitation. In: CVPR. pp. 3462–3471 (2020)
22. Kohavi, R., et al.: A study of cross-validation and bootstrap for accuracy estimation and model selection. In: IJCAI. pp. 1137–1145 (1995)

23. Li, B., Peng, X., Wang, Z., Xu, J., Feng, D.: Aod-net: All-in-one dehazing network. In: ICCV. pp. 4770–4778 (2017)
24. Li, B., Ren, W., Fu, D., Tao, D., Feng, D., Zeng, W., Wang, Z.: Benchmarking single-image dehazing and beyond. *IEEE TIP* **28**(1), 492–505 (2019)
25. Liu, R., Liu, J., Jiang, Z., Fan, X., Luo, Z.: A bilevel integrated model with data-driven layer ensemble for multi-modality image fusion. *IEEE TIP* **30**, 1261–1274 (2020)
26. Liu, X., Ma, Y., Shi, Z., Chen, J.: Griddehazenet: Attention-based multi-scale network for image dehazing. In: ICCV. pp. 7314–7323 (2019)
27. Liu, Z., Wei, P., Jiang, J., Cao, W., Bian, J., Chang, Y.: Mesa: Boost ensemble imbalanced learning with meta-sampler. *NeurIPS* **33** (2020)
28. Meng, G., Wang, Y., Duan, J., Xiang, S., Pan, C.: Efficient image dehazing with boundary constraint and contextual regularization. In: ICCV. pp. 617–624 (2013)
29. Mounsaveng, S., Laradji, I., Ben Ayed, I., Vázquez, D., Pedersoli, M.: Learning data augmentation with online bilevel optimization for image classification. In: *WACV*. pp. 1691–1700 (2021)
30. Narasimhan, S.G., Nayar, S.K.: Chromatic framework for vision in bad weather. In: *CVPR*. pp. 598–605 (2000)
31. Narasimhan, S.G., Nayar, S.K.: Vision and the atmosphere. *IJCV* **48**(3), 233–254 (2002)
32. Qin, X., Wang, Z., Bai, Y., Xie, X., Jia, H.: Ffa-net: Feature fusion attention network for single image dehazing. In: *AAAI*. pp. 11908–11915 (2020)
33. Qu, Y., Chen, Y., Huang, J., Xie, Y.: Enhanced pix2pix dehazing network. In: *CVPR*. pp. 8160–8168 (2019)
34. Ren, W., Liu, S., Zhang, H., Pan, J., Cao, X., Yang, M.H.: Single image dehazing via multi-scale convolutional neural networks. In: *ECCV*. pp. 154–169 (2016)
35. Ren, W., Ma, L., Zhang, J., Pan, J., Cao, X., Liu, W., Yang, M.H.: Gated fusion network for single image dehazing. In: *CVPR*. pp. 3253–3261 (2018)
36. Shao, Y., Li, L., Ren, W., Gao, C., Sang, N.: Domain adaptation for image dehazing. In: *CVPR*. pp. 2808–2817 (2020)
37. Shu, J., Xie, Q., Yi, L., Zhao, Q., Zhou, S., Xu, Z., Meng, D.: Meta-weight-net: Learning an explicit mapping for sample weighting. *arXiv preprint arXiv:1902.07379* (2019)
38. Silver, D., Lever, G., Heess, N., Degris, T., Wierstra, D., Riedmiller, M.: Deterministic policy gradient algorithms. In: *ICML*. pp. 387–395 (2014)
39. Sun, M., Dou, H., Li, B., Yan, J., Ouyang, W., Cui, L.: Autosampling: Search for effective data sampling schedules. In: *ICML*. pp. 9923–9933 (2021)
40. Sutton, R.S., McAllester, D.A., Singh, S.P., Mansour, Y.: Policy gradient methods for reinforcement learning with function approximation. In: *NeurIPS*. pp. 1057–1063 (2000)
41. Tian, K., Lin, C., Sun, M., Zhou, L., Yan, J., Ouyang, W.: Improving auto-augment via augmentation-wise weight sharing. *arXiv preprint arXiv:2009.14737* (2020)
42. Wang, X., Pham, H., Michel, P., Anastasopoulos, A., Carbonell, J., Neubig, G.: Optimizing data usage via differentiable rewards. In: *ICML*. pp. 9983–9995 (2020)
43. Wu, H., Qu, Y., Lin, S., Zhou, J., Qiao, R., Zhang, Z., Xie, Y., Ma, L.: Contrastive learning for compact single image dehazing. In: *CVPR*. pp. 10551–10560 (2021)
44. Wu, X., Wang, L., Xia, Y., Liu, W., Wu, L., Xie, S., Qin, T., Liu, T.Y.: Temporally correlated task scheduling for sequence learning. In: *ICML*. pp. 11274–11284 (2021)
45. Zhang, H., Patel, V.M.: Densely connected pyramid dehazing network. In: *CVPR*. pp. 3194–3203 (2018)

46. Zheng, Z., Ren, W., Cao, X., Hu, X., Wang, T., Song, F., Jia, X.: Ultra-high-definition image dehazing via multi-guided bilateral learning. In: CVPR. pp. 16180–16189 (2021)
47. Zhu, Q., Mai, J., Shao, L.: A fast single image haze removal algorithm using color attenuation prior. *IEEE TIP* **24**(11), 3522–3533 (2015)